Statistical electric field and switching time distributions in PZT 1Nb2Sr ceramics: Crystal- and microstructure effects

Sergey Zhukov, Hans Kungl, Yuri A. Genenko, and Heinz von Seggern

Citation: Journal of Applied Physics **115**, 014103 (2014); doi: 10.1063/1.4860335
View online: http://dx.doi.org/10.1063/1.4860335
View Table of Contents: http://scitation.aip.org/content/aip/journal/jap/115/1?ver=pdfcov
Published by the AIP Publishing

Statistical electric field and switching time distributions in PZT 1Nb2Sr ceramics: Crystal- and microstructure effects

Sergey Zhukov,[1,a] Hans Kungl,[2,3] Yuri A. Genenko,[1] and Heinz von Seggern[1]
[1]*Institut für Materialwissenschaft, Technische Universität Darmstadt, Alarich-Weiss-Straße 2, 64287 Darmstadt, Germany*
[2]*Forschungszentrum Jülich, Institut für Energie- und Klimaforschung IEK-9, 52425 Jülich, Germany*
[3]*Institut für Angewandte Materialien–Keramik in Maschinenbau, Karlsruher Institut für Technologie, 76131 Karlsruhe, Germany*

(Received 28 September 2013; accepted 14 December 2013; published online 6 January 2014)

Dispersive polarization response of ferroelectric PZT ceramics is analyzed assuming the inhomogeneous field mechanism of polarization switching. In terms of this model, the local polarization switching proceeds according to the Kolmogorov-Avrami-Ishibashi scenario with the switching time determined by the local electric field. As a result, the total polarization reversal is dominated by the statistical distribution of the local field magnitudes. Microscopic parameters of this model (the high-field switching time and the activation field) as well as the statistical field and consequent switching time distributions due to disorder at a mesoscopic scale can be directly determined from a set of experiments measuring the time dependence of the total polarization switching, when applying electric fields of different magnitudes. PZT 1Nb2Sr ceramics with Zr/Ti ratios 51.5/48.5, 52.25/47.75, and 60/40 with four different grain sizes each were analyzed following this approach. Pronounced differences of field and switching time distributions were found depending on the Zr/Ti ratios. Varying grain size also affects polarization reversal parameters, but in another way. The field distributions remain almost constant with grain size whereas switching times and activation field tend to decrease with increasing grain size. The quantitative changes of the latter parameters with grain size are very different depending on composition. The origin of the effects on the field and switching time distributions are related to differences in structural and microstructural characteristics of the materials and are discussed with respect to the hysteresis loops observed under bipolar electrical cycling. © *2014 AIP Publishing LLC*. [http://dx.doi.org/10.1063/1.4860335]

I. INTRODUCTION

A constitutive feature, that distinguishes a ferroelectric from a non-ferroelectric piezoelectric material, is the property that by means of sufficiently high temporary electric fields a persistent remanent polarization can be induced, which can be reversed when electric fields in the opposite direction are applied. The dynamics of the switching process is an important element in the description and understanding of ferroelectric materials which is relevant to microelectronic[1] and micromechanical[2] applications. Two basic concepts describing mechanisms of the polarization reversal behaviour have been established. The Kolmogorov-Avrami-Ishibashi (KAI) type based models stress the time dependence of the (microscopic) processes underlying the polarization switching which occurs uniformly in a system subject to the mean electric field.[3–10] Nucleation and growth of reversed domains are alternatively considered to both require time to become effective for domain switching and related polarization reversal. The second concept favours models, comprising the statistical approach,[11–20] which are based on the assumption that conditions for switching given by the local environment are different in different areas of the ceramics, which leads to a distribution of switching times. The feature common to these models can be summarized by the intrinsic randomness (IR) of the local conditions for switching. The first consistent formulation of the latter approach called the nucleation limited switching (NLS) model was suggested by Tagantsev *et al.*[11]

The main difference between the distinct statistical IR models is the degree in which they try to trace back the randomness to their physical origin, which may be either due to differences in the intention or to different stages of development of the models. The original NLS model, in accordance with the label "non-Kolmogorov-Avrami switching kinetics" used in the title of the pioneering publication, in first instance seems to be designed to show that there are alternatives to the KAI model, which match the experimental observations much better than the KAI model. In this model, the randomly distributed variables are the switching times with the physical origin of their randomness left as a completely black box. In the follow-up publication,[21] however, the same group considered a surface-stimulated nucleation mechanism of reverse domains, characteristic of the film geometry, which results in an exponentially wide distribution of waiting times, the term coined by Tagantsev *et al.*[11] In the works,[12,19,22] local random electric fields due to randomly distributed point or dipole defects were considered as a reason for the different local switching conditions. Accordingly, the Lorentzian distribution of local random fields was used to describe the polarization reversal in thin ferroelectric films.[12,16,17] Alternatively, a Gaussian distribution of local random fields was applied to describe the dispersive

[a]Author to whom correspondence should be addressed. Electronic mail: zhukov@e-mat.tu-darmstadt.de

polarization response of bulk ferroelectric ceramics.[23] Further development of the IR approach resulted in a concept, named the inhomogeneous field mechanism (IFM) model,[15,18] which leaves the form of the statistical field distribution a priori unspecified, while at the same time it provides a calculation scheme which allows for the computation of this distribution from the experimental data. In contrast to the other IR models,[12,16,17,19] the IFM model tries to relate the non-uniform switching behaviour to the random spatial distribution of the applied electric field. This procedure provides a chance to identify patterns in the field distributions that are typical for specific structural and microstructural features or the materials state and to correlate the shape and parameters of the field distribution with the materials characteristics. Additionally, this analysis allows for the investigation of the microscopic characteristics of the local polarization switching, such as the dependence of the local switching time $\tau(E)$ on the value of the local electric field E. The other details of the microscopic switching process are neglected in the IMF model by assuming that switching of a local region occurs instantly as soon as the poling time exceeds respective $\tau(E)$. An essential limitation of the IMF concept[15,18] and of the other IR models[12,16,17,19] is that the spatial random field distribution is assumed to be static thus neglecting contribution of the time-dependent depolarization fields which develop in the course of polarization switching. Recent self-consistent simulations of polarization switching in bulk polycrystalline ferroelectrics show, however, that account of field-mediated polarization correlations leads to a strong reduction of the local depolarization fields thus supporting the static IMF concept.[24]

The long term objective of this approach is to reduce the degree of randomness in the IR models by a stepwise integration of deterministic elements which describe relevant physical effects on the local electric fields and which could, in principle, be experimentally verified. The first attempt following the idea to extract the field distribution from switching curves after bipolar electrical fatigue and relating them to thereby initiated cracks was attempted by Zhukov *et al.*[14] A mathematically more sophisticated approach was offered soon after[15] being able to analyse the conditions that give rise to the distribution of fields by working out material specific differences within the framework of a universal switching behaviour.[18]

The present paper addresses the identification of effects of different crystallographic structures and a variation in grain sizes on the field distribution and other switching parameters. Within this work, switching experiments for tetragonal and rhombohedral PZT 1Nb2Sr ceramics with grain sizes ranging from 1 to 3 μm were performed. From the analysis following the IFM model, the characteristics of the field distribution and switching parameters depending on crystal structure and grain size will be identified and discussed in terms of the mechanisms leading to characteristic field distributions.

II. MATERIALS, EXPERIMENTAL DETAILS, AND DATA EVALUATION

A. Materials fabrication and characterization

Lead zirconate titanate samples doped with niobium and strontium corresponding to compositions $Pb_{0.975}Sr_{0.02}((Zr_xTi_{(1-x)})_{0.99}Nb_{0.01})O_3$ (x = 0.515, 0.5225, and 0.60) were prepared following a mixed oxide route[25] by means of attrition milling, drying the slurry in a rotation evaporator, and sieving the powder mixture. After calcinations at 850 °C/2 h, the powders were ball milled, dried, and finally sieved. Ceramics were sintered at four different temperatures, 975 °C, 1000 °C, 1050 °C, and 1100 °C, in order to adjust the grain size. Upper and lower temperature limit were given by the conditions to produce sufficiently dense materials without significant lead loss. Grain size and its dependence on the sintering temperature were quite similar for all three materials as demonstrated by SEM images (Leica Stereoscan 440) for the ceramics with the highest and the lowest Zr-content (Fig. 1). With density and grain size ranging roughly from 7.87 g/cm^3 and 1 μm when sintering at 975 °C

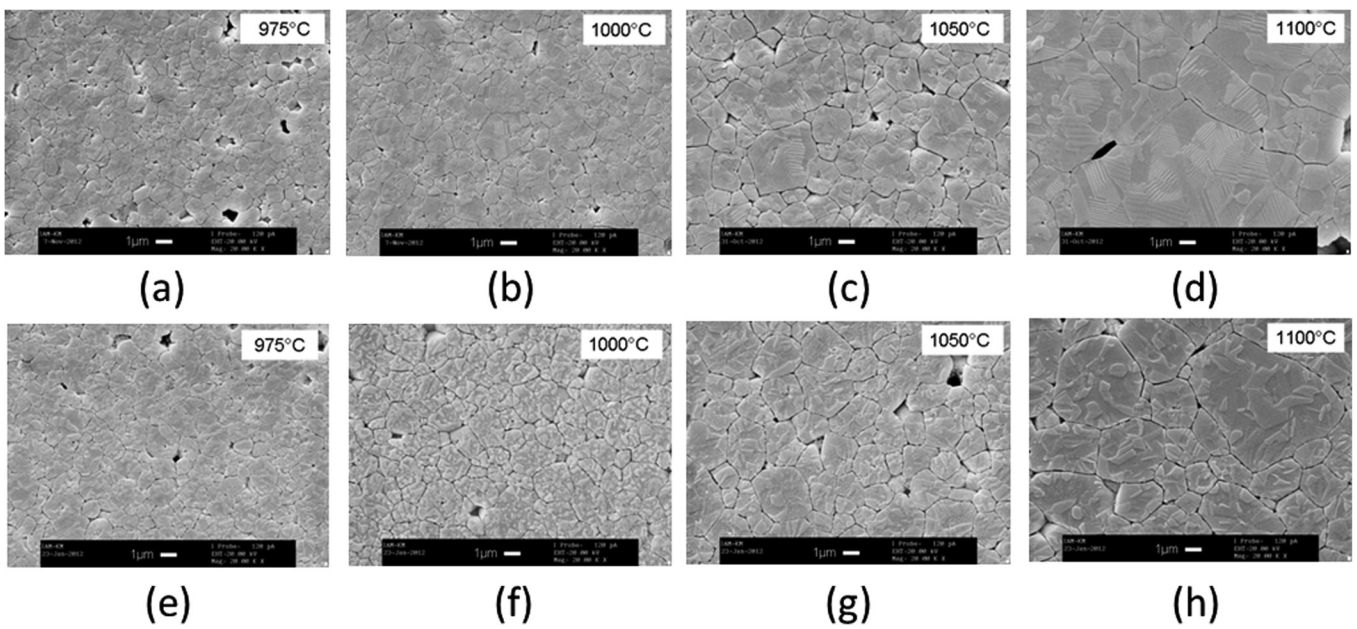

FIG. 1. SEM micrographs of PZT 51.5/48.5 1Nb2Sr (a)-(d) and PZT 60/40 1Nb2Sr (e)-(h) sintered at different temperatures as indicated.

TABLE I. Mean grain size and densities of PZT 1Nb2Sr ceramics sintered at temperatures 975 °C, 1000 °C, 1050 °C, and 1100 °C: specific compositions and average data.[26]

PZT 1Nb2Sr	975 °C	1000 °C	1050 °C	1100 °C
Grain size	μm	μm	μm	μm
51.5/48.5	1.01	1.20	1.56	2.94
52.25/47.75	1.18	1.20	1.75	3.10
60/40	1.12	1.29	1.89	2.65
Averages	1.16	1.33	1.81	3.14
Density	g/cm^3	g/cm^3	g/cm^3	g/cm^3
51.5/48.5	7.85	7.83	7.78	7.74
52.25/47.75	7.87	7.86	7.83	7.72
60/40	7.88	7.87	7.83	7.78
Averages	7.85	7.84	7.82	7.77

to 7.76 g/cm^3 and 3 μm when sintering at 1100 °C, both microstructural characteristics match the scope of previously analysed ceramics of the same type[26] (Table I).

As evidenced by diffraction patterns recorded with a Siemens D500 diffractometer at a wavelength of 1.5406 Å, PZT 51.5/48.5 1Nb2Sr is tetragonal and PZT 60/40 1Nb2Sr is rhombohedral. Only minor differences with sintering temperature are detectable for these materials, as shown for the 111 and 200 reflections for sintering temperatures of 975 °C and 1100 °C (Fig. 2). In the diffraction patterns of the PZT 52.75/47.25, one observes besides the typical tetragonal peaks additional diffraction intensity located in between the tetragonal 002 and 200 peaks, differing from those of the tetragonal microdomains. Several approaches have been suggested in order to explain the origin of this diffraction intensity: the presence of rhombohedral phase according to the conventional understanding of the morphotropic phase boundary (MPB),[26–28] the presence of monoclinic phase[29] and effects on diffraction patterns resulting from the presence of nanoscaled real structure[30,31] as well as variations of local lattice parameters owing to microstresses[32] and chemical inhomogeneity have been discussed. For a comparable PZT 1La material, the diffraction intensity between the tetragonal peaks has been attributed to the presence of nanostructured domains.[31,33] The PZT 52.25/47.75 1Nb2Sr will be referred as t-morphotropic in the text.

For the polarization switching experiments, disks are cut from the inner parts of a 9 to 10 mm diameter sintered body and were grounded and polished to 1.1 ± 0.1 mm thickness. Silver paint electrodes (Gwent) were applied on the faces and fired at 600 °C maximum temperature. Related bipolar polarization curves are presented in Fig. 3. High field electrical cycling experiments were carried out in a custom made measurement device for polarization and strain measurements.[34] The polarization and strain loops of the PZT 1Nb2Sr ceramics under bipolar electrical cycling at 25 mHz up to 3 kV/mm are shown in Fig. 3. With higher Zr-content, remanent polarization P_r increases, whereas coercive field E_c decreases (Figs. 3(a)–3(c)). For each composition, the characteristics of the polarization loops follow the same trend depending on grain size. Both, coercive field E_c and

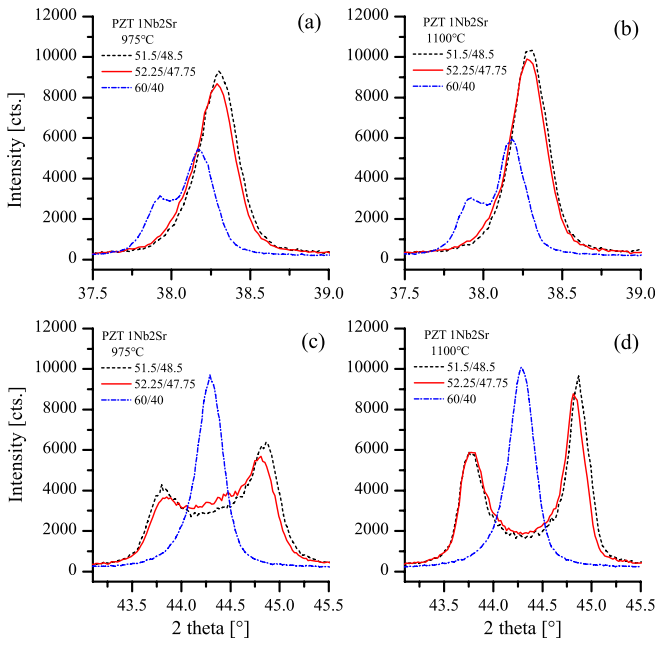

FIG. 2. X-ray reflections (111) (a) and (b) and (200) (c) and (d) of different PZT as indicated.

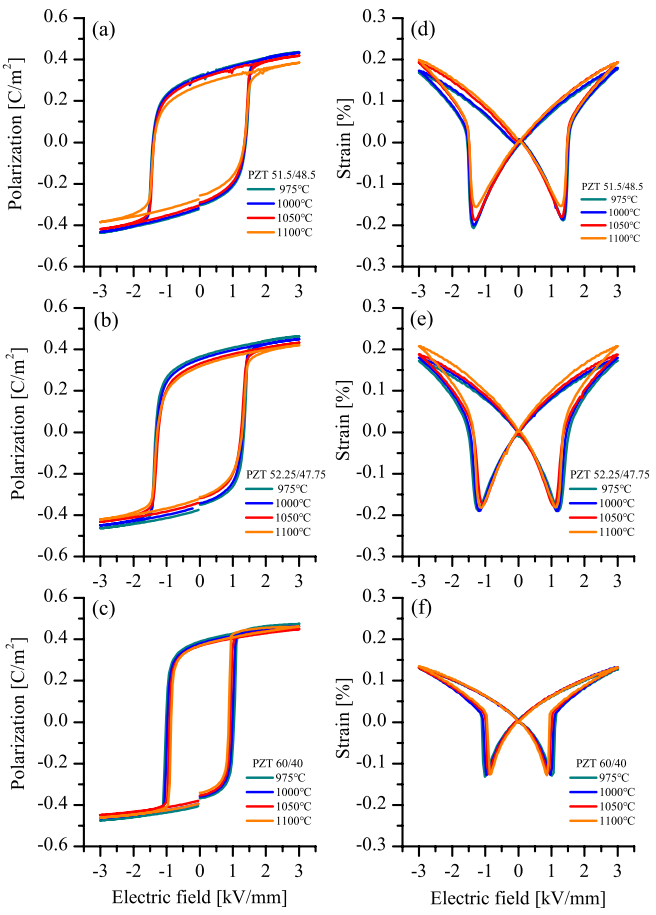

FIG. 3. Polarization hysteresis (a)-(c) and strain (d)-(f) for different PZT 1Nb2Sr as indicated.

remanent polarization P_r are lower for the ceramics with large grain size. While the changes in remanent polarization are quantitatively similar for all compositions, the effects of grain size on coercive fields are different. The tetragonal and t-morphotropic ceramics show only minor reductions in E_c with increasing grain size, whereas there is a pronounced decrease in E_c for the rhombohedral ceramics. Strain under bipolar cycles is higher for the tetragonal and t-morphotropic ceramics compared to the rhombohedral materials (Figs. 3(d)–3(f)).

B. Polarization switching experiments

The dynamic polarization measurements were carried out in a custom made device, consisting of a loading and a measurement circuit, which both had to be designed to allow an analysis over measurement times ranging from 1 μs to 100 s. The loading circuit consists of a voltage supply supported by a 1 μF buffer capacitor. It is connected via a fast push-pull switch from Behlke Co. (Germany) to the sample. In the measurement circuit, the voltage on a capacitor $C_0 = 4.4\ \mu$F and a 133 Ω resistor both in series with the sample was recorded, using a high impedance amplifier ($>10^{11}\Omega$) together with an oscilloscope (Tektronix TDS 510A). The time constant of the utilized electrical circuit was calculated to be about 200 ns taking the ferroelectric polarization of the sample into account. The resulting time constant was shorter than the shortest voltage pulse applied during the experiments. More details about the measurement setup can be found elsewhere.[14]

The temporal response of the reversed polarization ΔP at an applied electric field E_m was determined in four steps. At the first step, the sample was poled by a negative DC field of 2 kV/mm ($\sim 2E_C$) for 300 s followed by a short circuiting for 60 s assuring that the saturation polarization, P_S, was reached. At the second step, a positively directed switching field E_m was applied to the sample for a desired time t followed again by short circuiting recording the accumulated charge and therewith the electric displacement by the oscilloscope. During the third step, the sample was poled again for 300 s but this time by a positive DC field of 2 kV/mm to achieve its saturated $+P_S$ state. At the final fourth step, the forward poling on the fully poled sample was performed by applying the positive field E_m to the sample for a time period t for the second time. The recorded apparent electric displacement during forward poling contains all those components which exist in the switching experiment (step two) except for the switched ferroelectric polarization ΔP. Therefore, the net switched polarization $\Delta P(E_m, t)$ was calculated as the difference between the electric displacement values of switching and forward poling taken at time t after application of the electric field E_m.[14]

C. Data evaluation

The switching experiments provide a set of data which—from a formal point of view—correspond to a pointwise defined function $\Delta P(E_m, t)$ with the applied field E_m and the observation time t varying over a wide field range and time scale, respectively. Further data processing steps outlined in the flow diagram of Fig. 4, are explained in the following. One major objective of the calculation is to identify the statistical field distribution. Therefore, further analysis starts with the representation $\Delta P(E_m, t)$, so the data are displayed as a set of functions of the field E_m with different, but fixed t (the second step in the flow diagram). An important role in this description of the switching behaviour is given to $E_{\max}$, the electric field, at which—considering the fixed time—the maximum switching rate occurs. $E_{\max}$ is determined from the normalized logarithmic derivative of the functions $\Delta P(E_m, t)$ with respect to E_m (the third step in the flow diagram)

$$\Delta P_{\max}^{-1} E_m \partial \Delta P(E_m, t)/\partial E_m \equiv \Delta P_{\max}^{-1} \partial \Delta P(E_m, t)/\partial \ln E_m, \quad (1)$$

where $\Delta P_{\max}$ presents, in fact, the saturated value of the remnant polarization $2P_r$.

The logarithmic derivatives for different fixed times have a double functionality in the calculations. First, these functions are used to check if the essential conditions for applicability of the IFM model are fulfilled, i.e., the invariability (scaling) of the spatial field distribution with the level of the applied electric field. Necessary condition for this requirement is that the functions, when the field arguments are reduced to their specific maxima $E_{\max}(t)$ (the forth step in the flow diagram), all coincide within experimental error (ellipse area in the flow diagram), building thereby a dimensionless master curve $\Phi(E_m/E_{\max}(t))$ which can be regarded as a fingerprint of the system (see the left-hand stream in the flow diagram). Having a master curve established, the second role of the logarithmic derivatives can be exploited. Plotting the $E_{\max}$ values vs. the corresponding poling times t determines an experimental law for the analytical fitting (see the right-hand stream in the flow diagram). For the studied materials, the function of the form

$$E_{\max}(t) = E_0/[\ln(t/\tau_0)]^{1/\alpha} \quad (2)$$

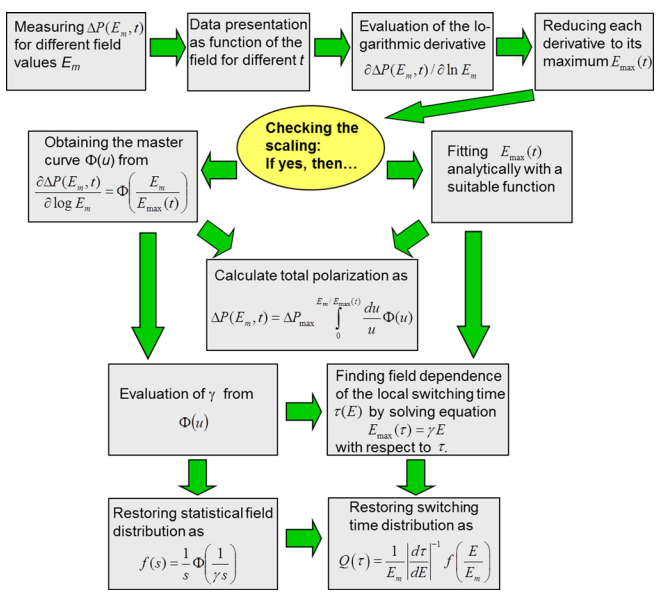

FIG. 4. Flow diagram of the dynamic switching data processing.

appears to be an adequate description so that the parameters τ_0, α, and E_0 can be determined by fitting the data set $(E_{\max}(t))$. Having determined $\Phi(E_m/E_{\max}(t))$ and the time dependence of $E_{\max}(t)$ in discrete or analytic form is sufficient to describe the macroscopic polarization response of the system[18] by the following equation (the central rectangle area in the flow diagram):

$$\Delta P(E_m, t) = \Delta P_{\max} \int_0^{E_m/E_{\max}(t)} \Phi(u) du/u. \tag{3}$$

To get a deeper insight into the microscopic and macroscopic mechanisms of polarization switching, further information can be extracted from $\Phi(u)$ and $E_{\max}(t)$. The weighted statistical distribution of the local values of the electric field E, normalized to the applied field $f(E/E_m)$ appears to follow directly from the master curve[15,18] as

$$f(s) = s^{-1}\Phi(1/\gamma s) \tag{4}$$

(the rectangle area bottom left in the flow diagram).

Here, the coefficient γ is a parameter of the theory which can be determined from additional information on the system. γ has the meaning of a proportionality factor between two characteristic fields $E_{\max}(t)$ and $E_{th}(t)$, namely $\gamma = E_{\max}(t)/E_{th}(t)$, where the first term is the before derived maximum position of the logarithmic derivative of the total polarization and the second one is defined as the solution of the equation $\tau(E) = t$ with respect to E thus comprising the microscopic switching mechanism. From the normalization conditions imposed on the statistical distribution function $f(s)$, the parameter γ can be determined as[18]

$$\gamma = \langle \cos\theta \rangle \int_0^{\infty} du\, \Phi(u)/u^2 \tag{5}$$

with $\langle \cos\theta \rangle$ being the averaged polar angle of the electric field directions with respect to the direction of the applied field. The latter value cannot be separately determined from measurements of the total polarization $\Delta P(E_m, t)$ but can, in principle, be estimated as $\langle \cos\theta \rangle = \Delta P_{\max}/2P_s$ if the spontaneous polarization P_s for a certain material is known, e.g., from measurements on single crystals or highly oriented thin films. Since such knowledge on the present PZT 1Nb2Sr materials is still missing, $\langle \cos\theta \rangle$ will be set to unity in the following analysis. As soon as the parameter γ is obtained (the last but one rectangle area in the left-hand stream in the flow diagram), the field distribution (4) is known. The local switching time dependence on the field can also be found by solving the equation $E = E_{\max}(\tau)/\gamma$ with respect to τ using the Eq. (2) (the last but one rectangle area in the right-hand stream in the flow diagram) that results in a relation

$$\tau(E) = \tau_0 \exp\left[(E_a/E)^{\alpha}\right] \tag{6}$$

similar to the Merz law[35] where an activation field $E_a = E_0/\gamma$ was introduced.

Knowledge of the two above dependencies $f(s)$ and $\tau(E)$ allows for the determination of the weighted statistical distribution of switching times (the rectangle area bottom right in the flow diagram)

$$Q(\tau) = E_m^{-1} |d\tau/dE|^{-1} f(E/E_m) \tag{7}$$

or more convenient distribution of the logarithm of switching times $G(\ln\tau) = \tau Q(\tau)$. With the help of this distribution of times, the total polarization reversal can be represented, similar to NLS approach,[11] as superposition of local KAI-like contributions[5]

$$p(t, \tau) = 2P_s\{1 - \exp(-(t/\tau)^{\beta})\} \tag{8}$$

from spatial regions with different local switching times

$$\Delta P(E_m, t) = \langle \cos\theta \rangle \int_0^{\infty} d\tau\, Q(\tau) p(t, \tau), \tag{9}$$

where β is the Avrami constant consisting of integer values corresponding to the dimensionality of the growing polarization domains[5] (note the correction by the factor $\langle \cos\theta \rangle$ with respect to Eq. (19) of Ref. 18). In disordered systems exhibiting the above mentioned scaling properties, Eq. (9) is reduced to Eq. (3) by substituting the KAI function (8) with the Heaviside function $2P_s\theta(t - \tau)$.

III. RESULTS

The raw data from the polarization switching experiments for the PZT 51.5/48.5, PZT 52.25/47.75, and PZT 60/40 1Nb2Sr materials with four different grain sizes for each composition are displayed by symbols in Figs. 5(a)–5(l). These diagrams show the time dependent changes in polarization during polarization reversal when applying different electric field strengths inverse to the initial poling direction. In order to acquire data sets suitable for the above analysis, the lower bound for the electric fields is determined by the requirement to obtain a sufficient amount of switched polarization within a reasonable experimental time interval. Towards the upper field range, the time resolution of the experimental setup limits the poling field level to values, which still allow for an evaluation of time profiles.

Consequently, the range of fields applied to the different materials is adjusted to the material specific switching behavior. Nevertheless, first characteristic features indicating the differences in polarization reversal behavior between the different investigated materials can already be recognized from the polarization vs. time data in Figs. 5(a)–5(l) when comparing (i) the polarization switching profiles of the different materials and grain sizes at the same field level or (ii) considering the fields required for switching within a given time range. Hereby a rough evaluation of the switching behavior can be based on the data of the inflection points of the polarization vs. time curves on logarithmic time scale. As an example, a comparison of the time profiles for the polarization switching at the same field level, namely 1.4 kV/mm, shows pronounced differences between the materials: In the rhombohedral PZT 60/40 1Nb2Sr samples, major changes in ΔP prevail within a time range of

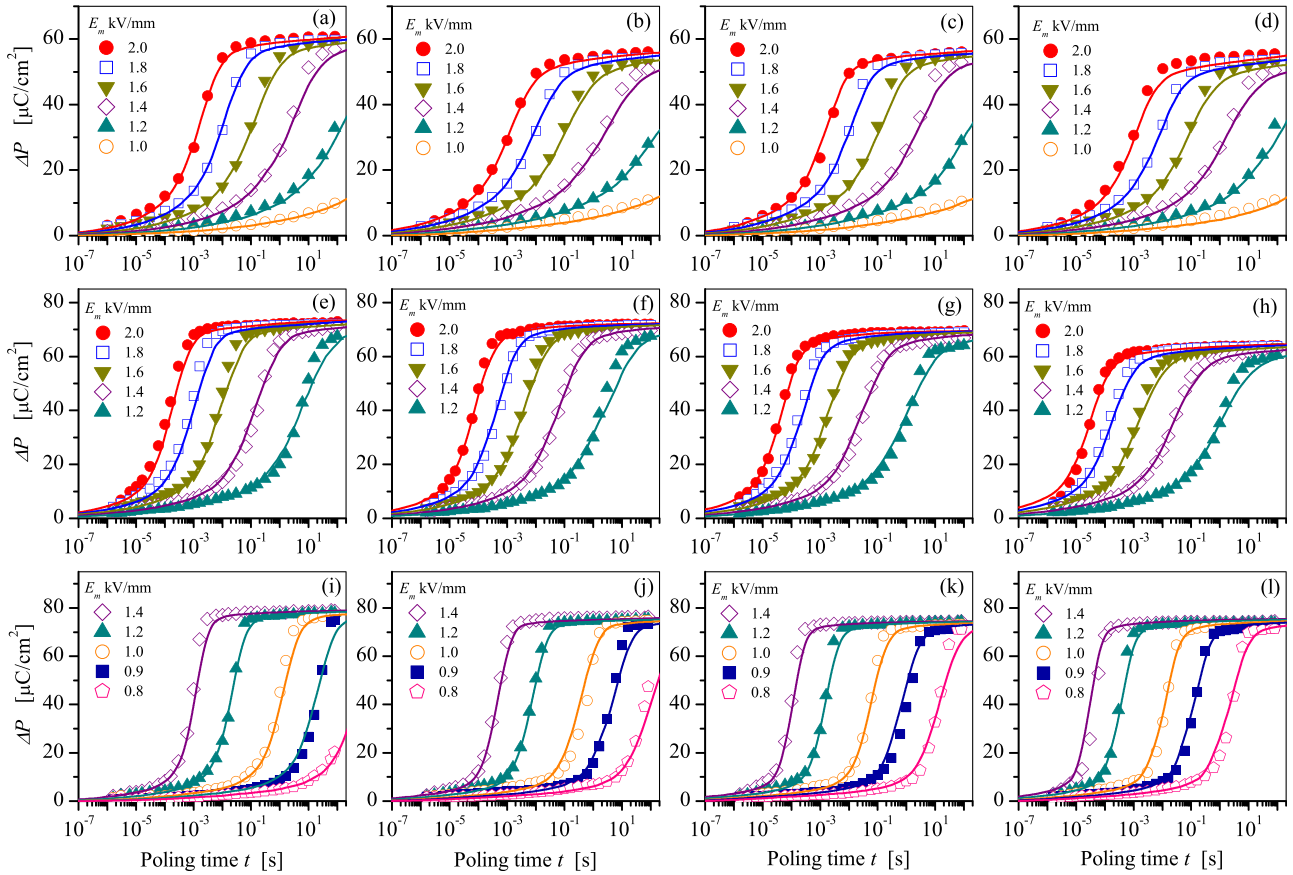

FIG. 5. (a)-(l) Switched polarization ΔP versus poling time t for different applied fields as indicated: PZT 51.5/48.5 1Nb2Sr with grain size: 1.01 μm (a), 1.20 μm (b), 1.56 μm (c), and 2.94 μm (d); PZT 52.25/47.75 1Nb2Sr with grain size: 1.18 μm (e), 1.20 μm (f), 1.75 μm (g), and 3.10 μm (h); PZT 60/40 1Nb2Sr with grain size: 1.12 μm (i), 1.29 μm (j), 1.89 μm (k), and 2.65 μm (l). Symbols correspond to the experimental results while the solid lines represent the field-related IFM model calculations by Eq. (3).

1 ms–10 ms. The switching times required to provide similar effects for the morphotropic and the tetragonal ceramics are much longer amounting to 10 ms to 1 s and 100 ms to 100 s for the PZT 52.25/47.75 1Nb2Sr and PZT 51.5/48.5 1Nb2Sr, respectively. On the other hand, focusing, e.g., to the time interval 1 ms to 100 ms, the fields required to result in pronounced switching are 1.6 to 1.8 kV/mm, 1.4 to 1.5 kV/mm, and 1.0 to 1.2 kV/mm for PZT 51.5/48.5 1Nb2Sr, PZT 52.25/47.75 1Nb2Sr, and PZT 60/40 1Nb2Sr, respectively. Both results indicate that switching of the rhombohedral PZT is much easier than for the other materials. Generally, for all materials the switching times are reduced with increasing applied electric field strengths. Comparing the switching time behavior on grain size for a given composition, the effects are much weaker. There is a trend toward decreasing switching times with increasing grain size, however, for a given composition and field the changes in switching times remain within one order of magnitude. While from the time profiles of polarization switching, some first ideas on qualitative composition dependent differences may be developed, a much more thorough evaluation according to the above describes IFM model will deliver much deeper insight.

Therefore, the data processing steps according to the evaluation procedure described in Sec. II C are illustrated in Figs. 6(a)–6(c) exemplarily for the PZT 51.5/48.5 1Nb2Sr ceramic with the mean grain size of 1.01 μm sintered at 975 °C. First, the $\Delta P(E_m = const, t)$ data sets (Fig. 5(a)) are converted to $\Delta P(E_m, t = const)$ and shown in Fig. 6(a). The normalized logarithmic derivative $\Delta P_{\max}^{-1} \partial \Delta P(E_m, t)/\partial \ln E_m$ from Eq. (1) derived by finite differences from the above discrete data for different observation times is presented in Fig. 6(b). This data representation shows that an electric field $E_{\max}(t)$ at which the maximum switching rate occurs exhibits a monotonic time dependence, whereby the lower the time t under consideration, the higher is the electric field $E_{\max}$ required for the maximum switching rate. All maxima thereby reach the same level within the experimental error as can be seen in Fig. 6(b). Plotting the normalized derivatives from Fig. 6(b) vs. the scaled field $E/E_{\max}(t)$ as depicted in Fig. 6(c), it becomes apparent that all norm derivatives at a given pulse duration time t coincide for different values of t. Thus, the conditions for applicability of the IFM model according to Genenko *et al.*[18] are fulfilled and the further analysis can be based on the master curves $\Phi(u)$ defined by the scaled logarithmic derivatives $\Delta P_{\max}^{-1} \partial \Delta P(E_m, t)/\partial \ln E_m$ as a function of $E/E_{\max}(t)$. The master curve behavior of the normalized logarithmic derivatives holds for each material class even for the different grain sizes; however, no universal master curve is obtained for all materials.

The respective results for $\Phi(u)$ are shown in Fig. 7. Depending on the Zr-content of the PZT, there are

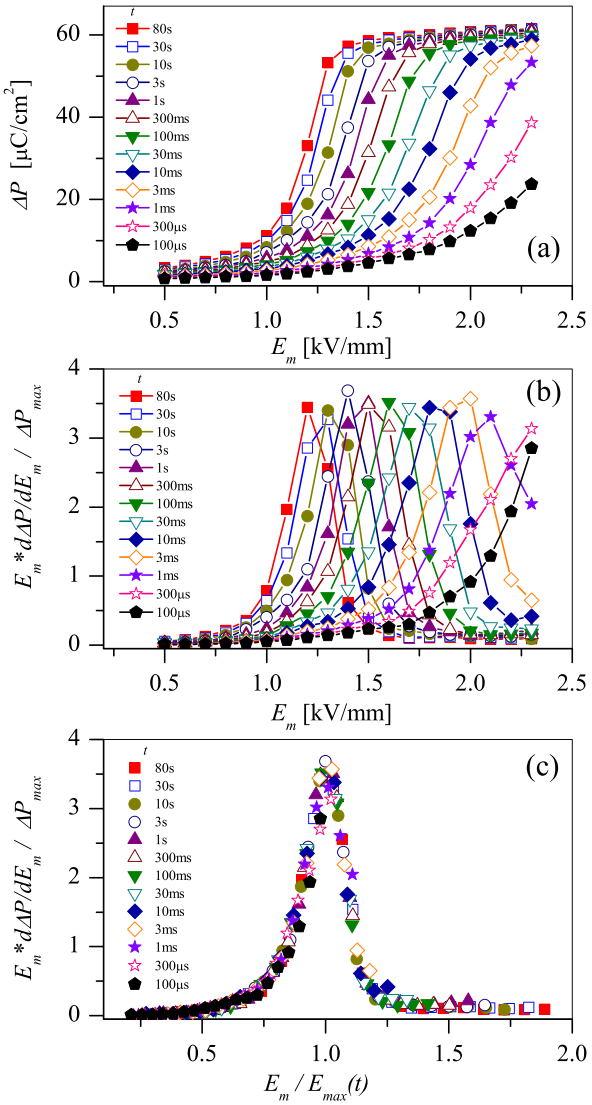

FIG. 6. Switched polarization vs. applied field E_m (a), normalized logarithmic derivative (b) and scaled normalized logarithmic derivative (c) at different poling pulse durations as indicated for the PZT 51.5/48.5 1Nb2Sr ceramic with the grain size of 1.01 μm.

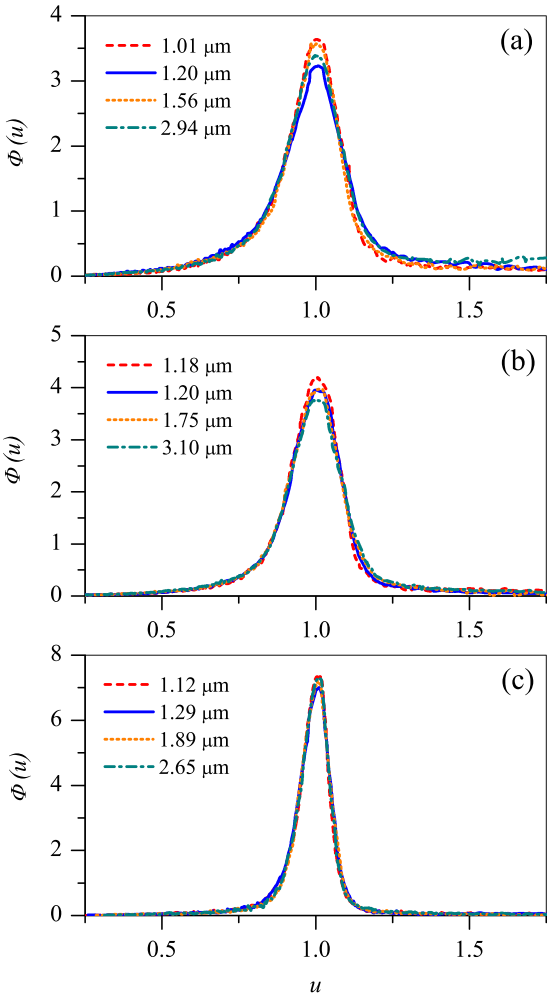

FIG. 7. Master curve Φ(u) for PZT 1Nb2Sr ceramics with different grain sizes as indicated: (a) PZT 51.5/48.5, (b) PZT 52.25/47.75, and (c) PZT 60/40.

pronounced differences in level and shape of $\Phi(u)$. Characteristic features of the master curves for PZT 51.5/48.5 1Nb2Sr and 52.25/47.75 1Nb2Sr are their relatively broad distribution and low values for their maxima located by definition of this function at $u = 1$. In contrast, the $\Phi(u)$ of the rhombohedral PZT 60/40 1Nb2Sr extends over a much smaller range with maximum values being roughly twice the values of the tetragonal and t-morphotropic materials. The full width at half maximum (FWHM) for the PZT 60/40 1Nb2Sr is less than 0.125, whereas for PZT 52.25/47.751Nb2Sr and PZT 51.5/48.5 1Nb2Sr the FWHM amounts to approximately 0.175 and 0.225, respectively. While there are pronounced differences with the Zr-content, at given composition, $\Phi(u)$ for different grain sizes remains essentially the same as can be seen in Fig. 7.

In Fig. 8, the characteristics of the $\tau(E)$ dependence of Eq. (2) with $\alpha = 1$ are shown. The fields at which maximum switching rate occurs are generally higher for the tetragonal PZT 51.5/48.5 1Nb2Sr and the PZT 52.25/47.75 1Nb2Sr than for the rhombohedral PZT 60/40 1Nb2Sr. While for the PZT 51.5/48.5 1Nb2Sr, E_{max} is not very sensitive to the variations in grain size, the materials with higher Zr/Ti ratio show a clear correlation of E_{max} decreasing with grain size increase. Most pronounced, in the rhombohedral PZT 60/40 1Nb2Sr ceramics, the difference in E_{max} between fine and coarse grained ceramics under fast switching conditions (i.e., high fields corresponding to short poling times) amounts up to 0.3 kV/mm. Under low field conditions (and corresponding high poling times), the difference between the fine and the coarse grained material reduces to less than half of this value. A similar trend with respect to the grain size dependence of E_{max} vs. t, even though quantitatively much less pronounced, holds also for the PZT 52.25/47.75 1Nb2Sr. For the PZT 51.5/47.5 1Nb2Sr, the differences with grain size are too small to conclude effects from consideration of their $E_{max}(t)$ plots. The results for the parameters τ_0, E_a and ΔP_{max} when fitting the E_{max} vs. t data according to Eq. (2) are shown in Fig. 9. The high-field switching times τ_0 are in the range of 10^{-11} s to 10^{-10} s for all materials. A trend common for all compositions is the decrease in the time τ_0 with increasing grain size. While for the PZT 51.5/48.5 1Nb2Sr,

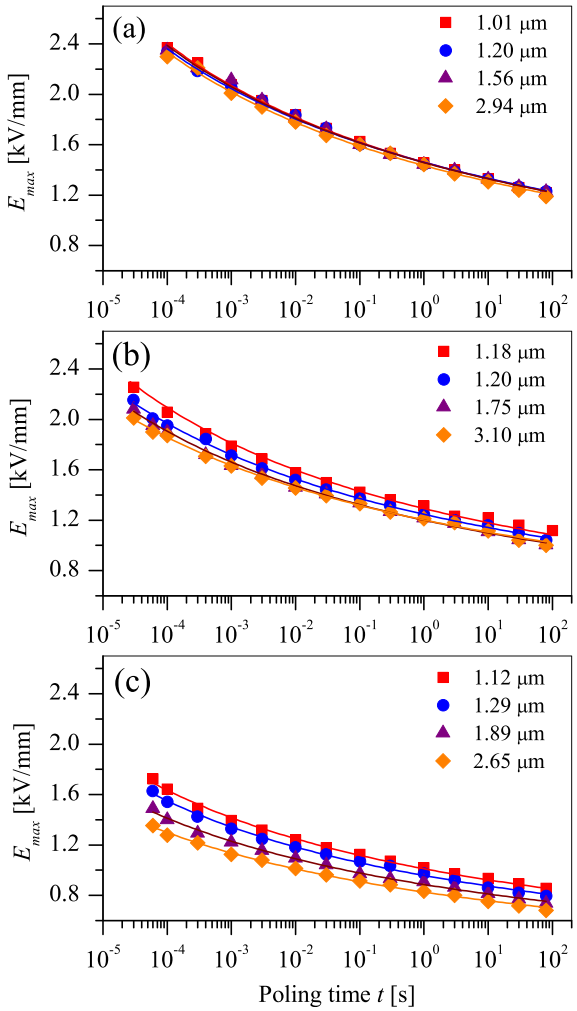

FIG. 8. E_{max} versus poling time t for PZT 1Nb2Sr ceramics with different grain sizes as indicated: (a) PZT 51.5/48.5, (b) PZT 52.25/47.75, and (c) PZT 60/40.

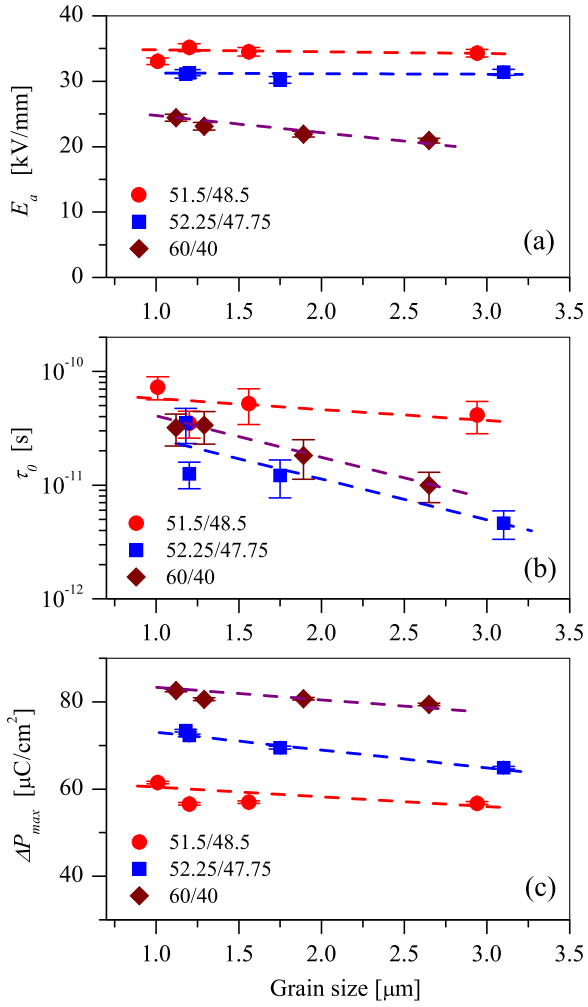

FIG. 9. Polarization switching characteristics for different PZT 1Nb2Sr as indicated: (a) activation field, (b) switching time and (c) polarization ΔP_{max}. Symbols correspond to the experimental data, whereas the dashed lines are guide for the eye.

τ_0 is reduced only very slightly along with increasing grain size, the decrease of τ_0 with grain size is very pronounced for the PZT 52.25/47.75 1Nb2Sr and PZT 60/40 1Nb2Sr. The activation fields E_a decrease with increasing Zr content of the PZT from 33 kV/mm for the PZT 51.5/48.5 1Nb2Sr to 25 kV/mm for the PZT 60/40 1Nb2Sr.

While E_a remains almost independent from grain size for the tetragonal and the t-morphotropic PZT 1Nb2Sr, the data for the rhombohedral materials show a distinct trend of decrease in the activation field with increasing grain size. The switchable polarization $\Delta P_{\max}$ increases with Zr-content from roughly 60 μC/cm^2 for the PZT 51.5/48.5 1Nb2Sr to 70 μC/cm^2 and 80 μC/cm^2 for the PZT 52.25/47.75 1Nb2Sr and PZT 60/40 1Nb2Sr, respectively. For all compositions, a slight decrease in $\Delta P_{\max}$ with grain size was detected.

The local field distributions for the PZT 51.5/48.5, 52.25/47.75, and 60/40 1Nb2Sr materials determined by Eq. (4) are presented in Fig. 10. These statistical field distributions indicate marked differences depending on the Zr-content in the materials. While broad distributions, spanning over a reduced field E/E_m range from roughly 0.625 to 1.25 with FWHM of $\delta E/E_m = 0.146$ and 0.107 were calculated for the PZT 51.5/48.5 and 52.25/47.75 1Nb2Sr materials, the width of the local field distribution is much narrower for the PZT 60/40 1Nb2Sr, extending from 0.75 to 1.125 with FWHM of $\delta E/E_m = 0.056$ only. There are only minor effects of grain size on the local field distributions. For the PZT 52.25/47.75 and 60/40 1Nb2Sr, the local field distribution functions almost coincide for all four levels of grain size. In the PZT 51.5/48.5 1Nb2Sr, the shape of the distribution remains essentially the same independent of grain size, however, in these materials calculations revealed slight shifts of the distributions which were not monotonic with increasing grain size.

The switching time distributions, Eq. (7), restored via the statistical field distributions, Eq. (4), and the local switching time dependence, Eq. (6), with $\alpha = 1$ are given in logarithmic representation $G(\ln(\tau/\tau_0)) = \tau Q(\tau)$ in Fig. 11 exemplarily for a field level of 1.5 kV/mm. The distribution of switching times is much narrower for the rhombohedral PZT 60/40 1Nb2Sr than for the tetragonal and the t–morphotropic materials. When evaluated on the logarithmic scale, the width of the distribution $\ln(\tau_{max}/\tau_{min})$ increases from 2.3 to 4.7 and 12.0 with decreasing Zr-content. Different behavior dependent on the Zr-content was also calculated with

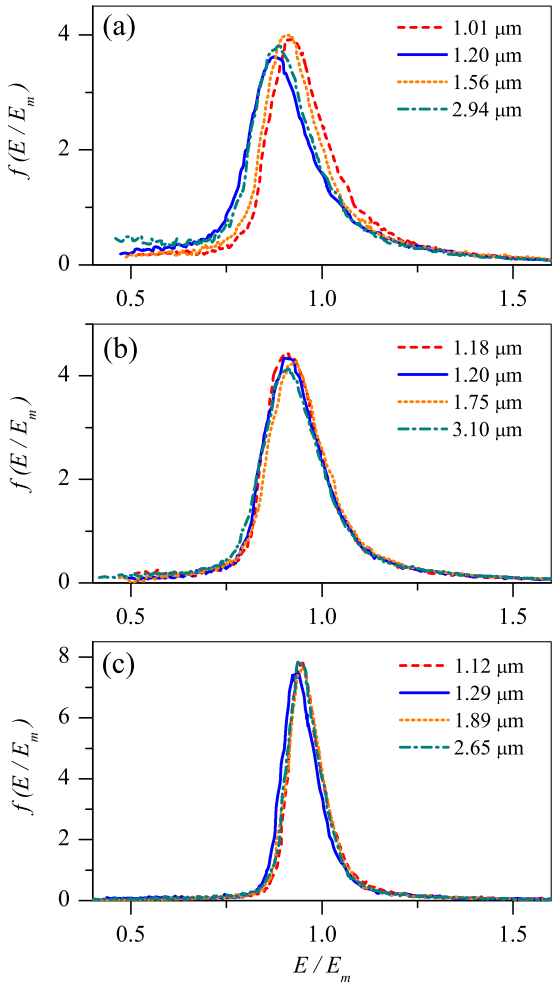

FIG. 10. Local field distributions for PZT 1Nb2Sr ceramics with different grain sizes as indicated: (a) PZT 51.5/48.5, (b) PZT 52.25/47.75, and (c) PZT 60/40.

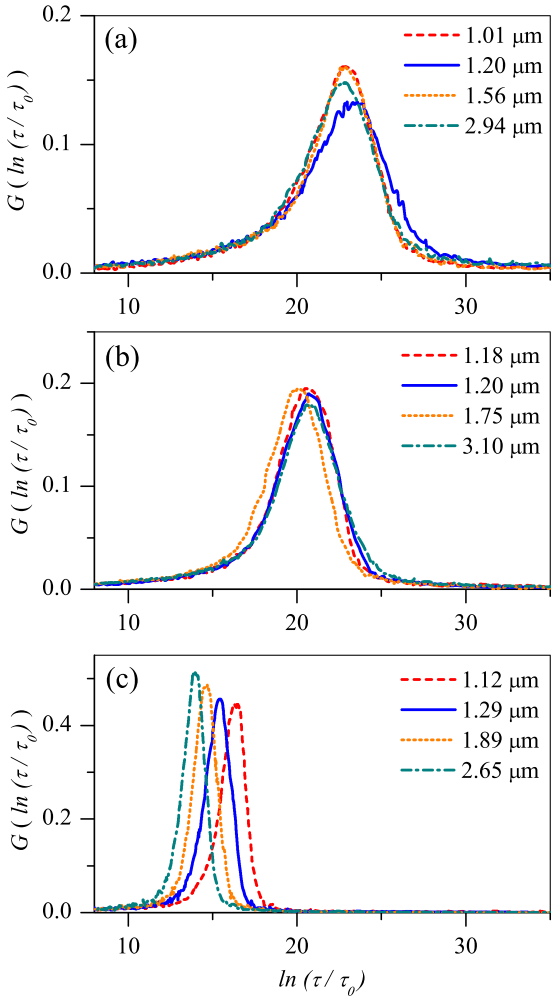

FIG. 11. Switching time distributions at $E_m = 1.5$ kV/mm for PZT 1Nb2Sr ceramics with different grain sizes as indicated: (a) PZT 51.5/48.5, (b) PZT 52.25/47.75, and (c) PZT 60/40.

respect to the grain size dependence of the switching time distributions. While the shape of the distributions remains essentially unaltered by grain size, there seem to be shifts on the time scale. In PZT 51.5/48.5, 52.25/47.75 1Nb2Sr materials exhibit only very slight inconsistent shifts of the time distributions.

In contrast to that, the rhombohedral materials show pronounced monotonic grain size dependence with respect to the time scale of the switching time distributions, shifting the maximum of the $G(\ln(\tau/\tau_0))$ distribution from approximately 18 to 16. With account of respective τ_0 magnitudes from Fig. 9(b) this corresponds to the change of the maximum position of $G(\ln(\tau/\tau_0))$ from $\tau = 2 \times 10^{-3}$ s to $\tau = 8 \times 10^{-5}$ s.

IV. DISCUSSION

Comparison of experimental results with formula (3) displayed by solid lines in Figs. 5(a)–5(l) exhibits good agreement with the dynamic switching data for materials of all compositions and grain sizes. However, the macroscopic and microscopic characteristics underlying the theoretical curves are remarkably distinct for different materials depending on both crystallographic symmetry of the studied compounds and their microstructural characteristics like grain size.

A. Variation of field distributions due to crystallographic features

One of the most interesting results derived from the experiments and the IFM analysis is the pronounced difference in the scope of field strengths at which switching occurs depending on composition as indicated by the shape and width of the master curve $\Phi(u)$ (Fig. 7) and the statistical field distribution $f(s)$ (Fig. 9). While for rhombohedral PZT 1Nb2Sr ceramics, the distribution is quite narrow, for tetragonal compositions the polarization switching extends over a wide field range. Thus, starting point for the discussion will be a brief reconsideration of the crystallographic and dielectric characteristics of tetragonal and rhombohedral PZT, before analyzing their effects on the field and time distributions.

Two major differences in crystallographic characteristics between tetragonal and rhombohedral materials are the number of polarization axes and the lattice distortion, i.e., the relative differences between the lattice constants in polarization direction compared to the nonpolarized direction.

There are 6 permissible polarization directions in the tetragonal PZT, whereas in the rhombohedral there are 8. The lattice distortion (c/a - 1) for tetragonal PZT is approximately 2%, whereas the corresponding value for rhombohedral PZT is only 0.7%.[36] Both small lattice distortion and high number of permissible polarization directions favor enhanced switching in rhombohedral PZT. Another parameter which distinguishes the two materials is the dielectric anisotropy, which is much lower in the rhombohedral PZT as is reflected by the properties of the dielectric tensor ε_{ik}. For example, the parameter of the anisotropy $\varepsilon_{11}/\varepsilon_{33}$ amounts to 4.5 for the tetragonal 50/50 PZT composition but abates to 1.8 for the rhombohedral 60/40 composition.[37]

These distinct features should have a great impact on the electrodynamic behavior of the compositions of different symmetry and on the distribution of electric fields. A thorough analysis of the impact of orientation distributions and dielectric anisotropy in polycrystalline PZT on the field distribution and their effects on polarization switching will be very complex; therefore, the discussion here is focused on the polarization switching behavior of specific orientations.

B. Comparison of switching in ceramics and oriented thin films

Although no switching data on single crystal PZT are available, important issues can be learned from measurements on highly oriented thin PZT films available for many compositions.[38–42] As well as in the case of (bulk) sintered PZT ceramics,[43] dielectric constant and electrical coupling in thin PZT films exhibit maximum for compositions near the MPB between the tetragonal and rhombohedral phases.[38–41] Thereby epitaxially grown thin films (200–300 nm) of {001} orientation possess a minimum value of the spontaneous polarization P_s at MPB[39] while the {111}-oriented films display maximum P_s and the remnant polarization P_r at MPB[40,41] thus revealing a great impact of texture on the ferroelectric properties. There are some discrepancies concerning the high-field saturated values of the spontaneous polarization P_s and the coercive field E_c in {111}-oriented films. From *P-E*-hysteresis loops at a frequency of 20 Hz and the maximum electric field strength of 25 kV/mm, strongly composition dependent P_s and P_r as well as the minimum value of E_c at MPB are reported by Oikawa *et al.*[40] On the other hand, *P-E*-hysteresis loops at the frequency of 1 Hz with the maximum electric field strength of 40 kV/mm reveal that the saturated value of P_s is composition independent, while E_c demonstrates monotonic decrease from the tetragonal towards the rhombohedral side as reported by Gerber *et al.*[41] The *P-E*-hysteresis loops become thereby increasingly slanted that means a decreasing P_r/P_s-ratio and smearing of the switching process on the field scale. Generally, smaller anisotropy and smaller lattice distortion facilitate easier domain reversal, which results in smaller coercive field strength E_c. Unique electromechanical and dielectric properties of PZT films around MPB are believed to be mostly determined by {111}-oriented domains.[40] An increasingly slanted form of the *P-E* loops for higher-Zr compositions was also observed by Jo *et al.*[42] at the measuring frequency of 2 kHz where it was related with generally easier switching at higher Zr contents.

The studied PZT ceramics exhibit both similar and distinct features with respect to thin oriented films. First note a distinct variation of polarization loops in the two materials: in the film case, they become more and more slanted with increasing Zr content while in the doped PZT ceramics they get a more rectangle form (Fig. 3). A related distinct feature is the behavior of the remnant polarization P_r. The high-field saturation value of P_s in oriented films is independent of composition and, hence, of the material symmetry though P_r in samples with higher Zr content are smaller due to back switching of the spontaneous polarization.[41,42] The latter property is not retained in Nb-Sr doped ceramics which exhibit an even more rectangular form of the loops for higher Zr content. Thereby the remnant polarization P_r remarkably increases with the higher Zr content (Fig. 9(c)). The differences in the polarization behavior between the mostly {111} oriented thin films and the polycrystalline PZT 1Nb2Sr ceramics may arise from different origins. First, the non-180° domain wall motion is inhibited in thin films[41] whereas pronounced switching of this type occurs in the ceramics. Thus, the contributions from non-180° switching may account for the composition dependent differences in P_s in the ceramics. Second, in thin films, stresses from the substrate are present.[39] These stresses, being high enough to influence even lattice parameters,[39] may be a major reason for the pronounced backswitching behavior and slanted polarization loops in thin films.

Another property, namely the reduction of the coercive field E_c with increasing Zr content is common for films and the present doped ceramics. Generally, high Zr containing rhombohedral materials in both film and ceramic forms exhibit a higher ratio of switched unit cells than tetragonal ones.[44,45] This is in favor of a narrower spatial distribution of principal axes of the random dielectric tensor ε_{ik} which approaches a uniform tensor and, consequently, produces a more uniform spatial field distribution. The latter is described by a statistical field distribution as in Fig. 10(c) which is narrower than those for the more tetragonal compositions in Figs. 10(a) and 10(b). Another reason for increasing homogeneity of the electric field with increasing Zr content on the rhombohedral compositional side is the above mentioned reduced anisotropy of the dielectric properties.

Note that field and time distributions in the doped PZT ceramics exhibit different changes with compositional variation than the {111}-oriented PZT films.[42] In films, both distributions become broader with increasing Zr content, that might be related to the above mentioned substrate effect, while in bulk samples they get narrower as is illustrated by Fig. 12. Differently from Jo *et al.*,[42] it is concluded that easier switching observed in both film and bulk samples with increasing Zr content is rather related to the decrease of the coercive field in both materials than to the variation of the switching time distribution. Generally, broadening of the switching time spectrum can hardly be interpreted as easier switching behavior since in this case a substantial part of the material consequently switches at very long poling times. Figure 12 clearly shows that switching times in the

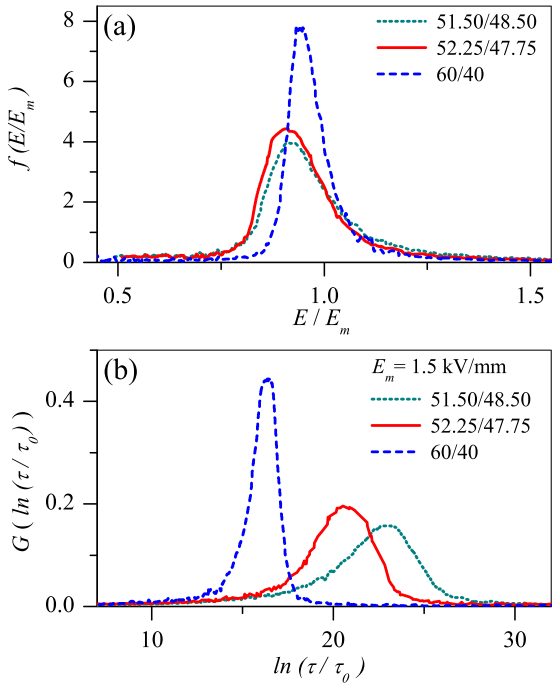

FIG. 12. Polarization switching distributions for different PZT 1Nb2Sr ceramics sintered at 975 °C as indicated: (a) local field distributions, (b) switching time distributions.

rhombohedral sample are by orders of the magnitude smaller than those in tetragonal ones even with the same grain size for the same applied field. At the same time, the distribution of switching times is much narrower in the rhombohedral case.

C. Grain size effect on macro- and microparameters of switching

The tetragonal and t-morphotropic compositions reveal only minor variation of the field and switching time distributions (Figs. 10(a), 10(b), 11(a), and 11(b)) with variation of the grain size. In contrast, rhombohedral materials exhibit monotonic reduction of the switching times with increasing grain size (Fig. 11(c)) though the corresponding statistical field distribution remains stable (Fig. 10(c)). This transformation clearly correlates with the corresponding reduction of the coercive field (Fig. 3) and the activation field E_a notable in Figs. 8(c) and 9(a). The latter may be explained by a higher sensitivity of the activation barrier to the grain size due to pinning at grain boundaries.[46] This barrier, related to the coercive field,[47,48] is apparently smaller in rhombohedral compositions (Fig. 3) due to the larger number of spatial polarization directions and the considerably smaller lattice distortion.[41] On the other hand, an enhanced clamping of the domain walls known in PZT ceramics with reduced grain size[46,49,50] may become influential compared to the smaller activation barrier; an effect less noticeable in predominantly tetragonal materials with higher switching barriers.

D. Direct and indirect ferroelastic effects on polarization switching

By both, the small lattice distortion and the higher number of permissible polarization directions enhanced switching in rhombohedral PZT is favored as discussed before. Although it is tempting to attribute the slower polarization process in the tetragonal PZT directly to the more difficult switching, care has to be taken to rely on this argument. The most pronounced differences in switching conditions depending on lattice parameter and more permissible switching directions result from mechanical stresses, which occur in particular for non-180° switching. Non-180° switching is the origin of changes in remanent strain after poling and therefore is in the focus of interest when considering the poling strain.

Contrary to that, a correlation between crystallographic characteristics and polarization changes has to take the contribution of both non-180° and 180° switching to polarization into account. There are two reasons that underline the quantitative importance of 180° switching with respect to its effects on polarization. First, the changes in polarization are higher for 180° switching than for non-180° switching. Moreover, the volume fractions of domains subject to 180° switching are considered much higher than those subject to non-180° switching.[45,51] The second point to be considered is the dependence of 180° polarization switching on the orientation of the domains. The driving force for switching the spontaneous polarization is related to the angle between the field vector and the vector of the spontaneous polarization. The higher the spontaneous polarization component inverse to the field direction, the higher is the switching rate.[52] Antiparallel orientations of a field vector and a spontaneous polarization vector imply high energy, so the release of this energy promotes the 180° switching.

As a consequence of the orientation dependence of 180° switching, the texture (i.e., the alignment of domains) in the poled state influences the macroscopic scale 180° switching. The 180° switching will be easier, if most domains are oriented close to antiparallel to the external field. A tentative explanation for the differences in polarization switching between tetragonal and rhombohedral PZT can be given based on the different degrees of domain alignment in the poled state. The theoretical distribution of orientations in a maximum poled rhombohedral PZT ceramics exhibit a narrower angular distribution of orientations than a tetragonal PZT. In the tetragonal PZT, the orientations lie within a conical angular range with a polar angle $\phi = \arcsin(\sqrt{2/3}) = 54.7°$ whereas in the rhombohedral PZT maximum poling results in orientations within a conical angular range with $\phi = (1/2)\arccos(1/3) = 35.3°$.[45] The differences in alignment of the domains between tetragonal and rhombohedral PZT will be even larger for the real poling state because of built-in electromechanical fields developing in a ferroelectric material as a result of the spatial electromechanical coupling of grains.[53] As evidenced from *in-situ* X-ray diffraction data, the distributions of orientations of domains after poling are much closer to the theoretically complete alignment for the rhombohedral than for the tetragonal PZT. Qualitatively, the higher degree of alignment can be also derived from the degree of poling which compares the theoretically calculated maximum poling strain.[45] The poling degree of tetragonal PZT 52.5/47.5 1La2Sr ceramics close to MPB is 0.26, whereas for PZT 55/45 1La2Sr, a material neighboring the

rhombohedral side of MPB the poling degree is 0.65.[36] Owing to the higher alignment of domain orientations resulting for a higher poling degree, the polarization switching distributions will be narrower.

With respect to a comparison between tetragonal and rhombohedral PZT, the major impact on polarization behavior is supposed to be related to these differences in alignment of domains in the poled state. However, the results on grain size dependence of the polarization behavior indicate that there are also other important factors of influence. In spite of higher poling degrees as indicated by the higher remanent strain[26] for fine grain sized PZT 1Nb2Sr, the polarization is faster for the coarse grained ceramics within each composition. Both, the differences in remanent strain and time behavior of polarization switching are, however, comparatively low. Therefore, the influence of grain size dependent field inhomogeneity, arising from the conditions at the grain boundaries may become more important. The misalignment of the neighboring grains with different orientations of the dielectric tensor as well as intergranular stresses lead to local modifications of the electric field vector. This together with the direct pinning of domain walls at grain boundaries affects the switching behavior in the grain boundary region.[53] In the fine grained ceramics, the volume fraction subject to this distribution of local fields will be higher. Thus, grain size dependent differences in polarization behavior may originate from the increasing field inhomogeneity caused by the large fraction of grain boundary area in fine grained ceramics.

Summarizing, the crystallographic characteristics of rhombohedral and tetragonal PZT cause different non-180° domain switching behavior owing to differences in associated mechanical stresses. In part, *direct* ferroelastic effects via enhanced non-180° domain switching contribute to the easier macroscopic polarization reversal of the rhombohedral PZT. However, more important for the macroscopic polarization reversal may be 180° switching, which depends on the initial configuration of the domains in the poled state. The alignment of domains in the remanent poled state—which again depends on ferroelastic characteristics—is higher for rhombohedral than for tetragonal PZT and thus provides more favorable conditions for 180° switching. This influence of the ferroelastic characteristics on polarization switching via 180° switching is an *indirect* one: they influence the texture of the domains, which in turn governs the 180° switching behavior.

V. CONCLUSIONS

In this experimental and theoretical study of polarization dynamics of PZT 1Nb2Sr ceramics of different crystallographic and microstructural properties, the questions what effects have the symmetry of phases and grain sizes on switching dynamics in different compounds have been treated. To this end, switching of spontaneous polarization was measured well below and above the respective coercive fields of different samples in the time domain between 1 μs and 100 s. Implementation of the IFM model of polarization switching allows insight in both macroscopic and microscopic characteristics of the polarization reversal. Statistical distributions of the local electric field values proved to be weakly dependent on the mean grain size but strongly dependent on the symmetry of the materials. Thus, in rhombohedral compositions—less anisotropic than tetragonal ones and possessing more options for polarization orientation—the field distributions become much narrower promoting more uniform spatial field distribution. This was followed by much more concentrated statistical switching time distributions. The latter distributions are also strongly affected by microscopic switching parameters such as the high-field switching time and the activation field. Both parameters were found to be remarkably smaller in more rhombohedral compositions exhibiting more pronounced descending grain size dependence. This results in a remarkable difference in switching time distributions making rhombohedral compositions two orders of the magnitude faster than tetragonal ones. Differently from the typical slanted polarization loops exhibited by thin oriented ferroelectric films of rhombohedral symmetry, the present doped PZT 1Nb2Sr ceramics reveal rectangular polarization loops for all compositions even more pronounced in the rhombohedral case. Although tetragonal materials are typically chosen for FeRAM applications for their high and stable remanent polarization P_r,[41] in the case of Nb-Sr doped materials the most suitable composition for this application seems to be the rhombohedral 60/40 one for its highest P_r magnitude and remarkably faster switching.

ACKNOWLEDGMENTS

The authors would like to thank the German Research Foundation (DFG) for its financial support in the framework of the Collaborative Research Center (SFB 595).

[1]J. F. Scott, *Ferroelectric Memories* (Springer, Berlin, 2000).
[2]P. Muralt, J. Micromech. Microeng. **10**, 136 (2000).
[3]A. N. Kolmogorov, Izv. Akad. Nauk, Ser. Math. **3**, 355 (1937).
[4]M. Avrami, J. Chem. Phys. **8**, 212 (1940).
[5]Y. Isibashi and Y. Takagi, J. Phys. Soc. Jpn. **31**, 506 (1971).
[6]V. Y. Shur, E. L. Rumyantsev, S. D. Makarov, and V. V. Volegov, Integr. Ferroelectr. **5**, 293 (1994).
[7]V. Y. Shur, E. L. Rumyantsev, S. D. Makarov, N. Y. Ponomarev, E. V. Nikolaeva, and E. I. Shishkin, Integr. Ferroelectr. **27**, 179 (1999).
[8]O. Lohse, M. Grossmann, U. Boettger, D. Bolten, and R. Waser, J. Appl. Phys. **89**, 2332 (2001).
[9]C. Verdier, D. C. Lupascu, H. von Seggern, and J. Rödel, Appl. Phys. Lett. **85**, 3211 (2004).
[10]D. C. Lupascu, S. Fedosov, C. Verdier, J. Rödel, and H. von Seggern, J. Appl. Phys. **95**, 1386 (2004).
[11]A. K. Tagantsev, I. Stolichnov, N. Setter, J. S. Cross, and M. Tsukada, Phys. Rev. B **66**, 214109 (2002).
[12]J. Y. Jo, H. S. Han, J.-G. Yoon, T. K. Song, S.-H. Kim, and T. W. Noh, Phys. Rev. Lett. **99**, 267602 (2007).
[13]S. Jesse, B. J. Rodriguez, S. Choudhury, A. P. Baddorf, I. Vrejoiu, D. Hesse, M. Alexe, E. A. Eliseev, A. N. Morozovska, J. Zhang, L.-Q. Chen, and S. Kalinin, Nature Mater. **7**, 209 (2008).
[14]S. Zhukov, S. Fedosov, J. Glaum, T. Granzow, Y. A. Genenko, and H. von Seggern, J. Appl. Phys. **108**, 014105 (2010).
[15]S. Zhukov, Y. A. Genenko, O. Hirsch, J. Glaum, T. Granzow, and H. von Seggern, Phys. Rev. B **82**, 014109 (2010).
[16]N. Dabra, J. S. Hundal, A. Nautiyal, K. C. Sekhar, and R. Nath, J. Appl. Phys. **108**, 024108 (2010).
[17]A. Nautiyal, K. C. Sekhar, N. P. Pathak, N. Dabra, J. S. Hundal, and R. Nath, Appl. Phys. A: Mater. Sci. Process. **99**, 941 (2010).

[18]Y. A. Genenko, S. Zhukov, S. V. Yampolskii, J. Schütrumpf, R. Dittmer, W. Jo, H. Kungl, M. J. Hoffmann, and H. von Seggern, Adv. Funct. Mater. **22**, 2058 (2012).
[19]D. Kedzierski, E. V. Kirichenko, and V. A. Stephanovich, Phys. Lett. A **375**, 685 (2011).
[20]S. Zhukov, Y. A. Genenko, M. Acosta, H. Humburg, W. Jo, J. Rödel, and H. von Seggern, Appl. Phys. Lett. **103**, 152904 (2013).
[21]G. Gerra, A. K. Tagantsev, and N. Setter, Phys. Rev. Lett. **94**, 107602 (2005).
[22]D. Viehland and J. F. Li, J. Appl. Phys. **90**, 2995 (2001).
[23]S. Zhukov, Y. A. Genenko, and H. von Seggern, J. Appl. Phys. **108**, 014106 (2010).
[24]Y. A. Genenko, J. Wehner, and H. von Seggern, J. Appl. Phys. **114**, 084101 (2013).
[25]M. Hammer and M. J. Hoffmann, J. Am. Ceram. Soc. **81**, 3277 (1998).
[26]H. Kungl and M. J. Hoffmann, J. Appl. Phys. **107**, 054111 (2010).
[27]B. Jaffee, W. R. Cook, and H. Jaffee, *Piezoelectric Ceramics* (R.A.N. Publishers, Marietta, OH, 1971).
[28]W. Wersing, W. Rossner, G. Eckstein, and G. Tomandl, Silicates Industriels **50**, 41 (1985).
[29]B. Noheda, D. E. Cox, G. Shirane, R. Guo, B. Jones, and L. E. Cross, Phys. Rev. B **63**, 014103 (2000).
[30]Y. M. Jin, Y. U. Wang, A. Khatchaturyan, J. F. Li, and D. Viehland, Phys. Rev. Lett. **91**, 197601 (2003).
[31]K. A. Schoenau, L. A. Schmitt, M. Knapp, H. Fuess, R. Eichel, H. Kungl, and M. J. Hoffmann, Phys. Rev. B **75**, 184117 (2007).
[32]I. MacLaren, L. A. Schmitt, H. Fuess, H. Kungl, and M. J. Hoffmann, J. Appl. Phys. **97**, 094102 (2005).
[33]M. Hinterstein, K. A. Schoenau, J. Kling, H. Fuess, M. Knapp, H. Kungl, and M. J. Hoffmann, J. Appl. Phys. **108**, 024110 (2010).
[34]H. Kungl and M. J. Hoffmann, Sens. Actuators, A **144**, 328 (2008).
[35]W. J. Merz, Phys. Rev. **95**, 690 (1954).
[36]H. Kungl, R. Theissmann, M. Knapp, C. Baehtz, H. Fuess, S. Wagner, T. Fett, and M. J. Hoffmann, Acta Mater. **55**, 1849 (2007).
[37]M. J. Haun, E. Furman, S. J. Jang, and L. E. Cross, Ferroelectrics **99**, 63 (1989).
[38]T. Yamamoto, Jpn. J. Appl. Phys., **35**, 5104 (1996).
[39]T. Oikawa, M. Aratani, K. Saito, and H. Funakubo, J. Cryst. Growth **237**, 455 (2002).
[40]T. Oikawa, M. Aratani, and H. Funakubo, J. Appl. Phys. **95**, 3111 (2004).
[41]P. Gerber, U. Böttger, and R. Waser, J. Appl. Phys. **100**, 124105 (2006).
[42]J. Y. Jo, S. M. Yang, H. S. Han, D. J. Kim, W. S. Choi, T. W. Noh, T. K. Song, J.-G. Yoon, C. Y. Koo, J.-H. Cheon, and S.-H. Kim, Appl. Phys. Lett **92**, 012917 (2008).
[43]B. Jaffe, R. S. Roth, and S. Marzullo, J. Appl. Phys. **25**, 809 (1954).
[44]J. L. Jones, M. Hoffman, and K. J. Bowman, J. Appl. Phys. **98**, 024115 (2005).
[45]N. Uchida and T. Ikeda, Jpn. J. Appl. Phys., Part 1 **6**, 1079 (1967).
[46]J. Petzelt, Ferroelectrics **400**, 117 (2010).
[47]M. Vopsaroiu, J. Blackburn, M. G. Cain, and P. M. Weaver, Phys. Rev. B **82**, 024109 (2010).
[48]M. Vopsaroiu, P. M. Weaver, M. G. Cain, M. J. Reece, and K. B. Chong, IEEE Trans. Ultrason. Ferroelectr. Freq. Control **58**, 1867 (2011).
[49]G. Arlt, Ferroelectrics **104**, 217 (1990).
[50]J. Glaum, Y. A. Genenko, H. Kungl, L. A. Schmitt, and T. Granzow, J. Appl. Phys. **112**, 034103 (2012).
[51]T. Ogawa, Y. Takeshita, T. Miyamoto, and D. I. Chun, Ferroelectrics **186**, 119 (1996).
[52]K. B. Chong, F. Guiu, and M. J. Reece, J. Appl. Phys. **103**, 014101 (2008).
[53]E. M. Anton, R. E. Garcia, T. S. Key, J. E. Blendell, and K. J. Bowman, J. Appl. Phys. **105**, 024107 (2009).